The Multiple-Vortex Nature of Tropical Cyclogenesis

JASON A. SIPPEL AND JOHN W. NIELSEN-GAMMON

Department of Atmospheric Sciences, Texas A&M University, College Station, Texas

STEPHEN E. ALLEN

National Weather Service Houston/Galveston, Dickinson, Texas

(Manuscript received 18 February 2005, in final form 2 November 2005)

ABSTRACT

This study explores the extent to which potential vorticity (PV) generation and superposition were relevant on a variety of scales during the genesis of Tropical Storm Allison. Allison formed close to shore, and the combination of continuous Doppler radar, satellite, aircraft, and surface observations allows for the examination of tropical cyclogenesis in great detail.

Preceding Allison's genesis, PV superposition on the large scale created an environment where decreased vertical shear and increased instability, surface fluxes, and low-level cyclonic vorticity coexisted. This presented a favorable environment for meso-α-scale PV production by widespread convection and led to the formation of surface-based, meso-β-scale vortices [termed convective burst vortices (CBVs)]. The CBVs seemed to form in association with intense bursts of convection and rotated around each other within the meso-α circulation field. One CBV eventually superposed with a mesoscale convective vortex (MCV), resulting in a more concentrated surface vortex with stronger pressure gradients.

The unstable, vorticity-rich environment was also favorable for the development of even smaller, meso-γ-scale vortices that formed within the cores of deep convective cells. Several meso-γ-scale convective vortices were present in the immediate vicinity when a CBV developed, and the smaller vortices may have contributed to the formation of the CBV. The convection associated with the meso-γ vortices also fed PV into existing CBVs.

Much of the vortex behavior observed in Allison has been documented or simulated in studies of other tropical cyclones. Multiscale vortex formation and interaction may be a common aspect of many tropical cyclogenesis events.

1. Introduction

Tropical cyclone track forecasts have improved considerably during the past 50 years, and while intensity forecast skill has lagged somewhat (DeMaria and Gross 2003), cyclogenesis forecasts have proven to be more difficult. Although the scientific and operational communities now understand which environments are favorable for tropical cyclone formation (e.g., Gray 1968, 1975; McBride and Zehr 1981), the ability to accurately forecast the evolution from a tropical disturbance to a tropical cyclone remains a challenge (Emanuel 2003). Hindering forecast skill improvement is an inadequate understanding of the early stages of tropical cyclogenesis.

Air–sea interaction instability theory (Emanuel 1986; Rotunno and Emanuel 1987), renamed wind-induced surface heat exchange (WISHE; e.g., Emanuel et al. 1994), has been accepted as the leading explanation for the maintenance and intensification of existing tropical cyclones (Craig and Gray 1996). The premise of this theory is that a positive feedback between oceanic heat fluxes and wind speed can largely explain tropical cyclone intensification. Given a vortex, the winds near the surface enhance fluxes of sensible and latent heat. This leads to more vigorous convection, stronger diabatic heating, and ultimately a stronger surface cyclone. The cycle completes as the stronger surface winds lead to even greater heat fluxes. While this theory adequately describes cyclone maintenance and intensification, an initial vortex of sufficient amplitude is needed to allow

Corresponding author address: Jason A. Sippel, Department of Atmospheric Sciences, Texas A&M University, 3150 TAMU, College Station, TX 77843.
E-mail: jsipp@ariel.met.tamu.edu

the feedback to proceed efficiently (Rotunno and Emanuel 1987; Emanuel 1989). The challenge is to predict when or whether an incipient disturbance will attain sufficient intensity and organization to allow WISHE to take over.

When discussing dynamical evolution, a consistent conceptual framework is essential. Many observational and numerical studies that have shed light on the initial stage of tropical cyclogenesis have used a potential vorticity (PV) perspective. PV thinking (Hoskins et al. 1985) is useful for several reasons. Because PV thinking describes the balanced portion of atmospheric flow and thermal structure, balanced vortices necessarily include anomalous PV. Also, because PV is a conserved quantity for all but diabatic and frictional processes, it can more easily be used to study vortex superposition than nonconserved quantities such as vorticity. For these reasons we choose the PV framework in this study. For more information on basic PV terminology and concepts see the appendix.

This article explores the extent to which the process of PV generation and superposition are relevant across many scales of motion during tropical cyclogenesis. This paradigm, which is consistent with both old and new ideas about tropical cyclogenesis and intensification, views tropical cyclone formation as involving the multiscale growth and superposition of multiple PV anomalies.

The superposition of synoptic-scale or large mesoscale [O(100 km) to O(1000 km)] positive PV anomalies is one possible mechanism for establishing the initial background disturbance needed for tropical cyclone formation. The thermal structure of an upper-level positive PV anomaly (e.g., Hoskins et al. 1985) is such that the atmosphere below it will be more favorable for surface-based convection. When upper- and lower-level positive PV anomalies superpose, the strengthened cyclonic circulation at the surface increases the surface fluxes of latent and sensible heat (e.g., Molinari et al. 1998). Deep convection and elevated low-level vorticity are climatological precursors of tropical cyclone development (e.g., Gray 1968, 1975; McBride and Zehr 1981), and the presence of both of these in an otherwise favorable environment can begin tropical cyclogenesis.

The paradigm followed in this paper also agrees well with the previous theory regarding smaller scales of tropical cyclone formation. For example, it is well known that large mesoscale convective systems (MCSs) often precede tropical cyclone formation (McBride and Zehr 1981). The mesoscale convective vortices (MCVs) that form within these convective systems (Menard and Fritsch 1989; Raymond and Jiang 1990; Chen and Frank 1993; Fritsch et al. 1994) can merge to form stronger, deeper, and wider circulations than those associated with the individual vortices. This type of PV superposition thus also enhances low-level vorticity and can thereby strengthen a tropical disturbance (e.g., Harr et al. 1996; Simpson et al. 1997; Ritchie and Holland 1997).

The ideas presented here are also consistent with those presented by Hendricks et al. (2004) and Montgomery et al. (2006). Those modeling studies showed that the system-scale toroidal circulation generated by deep convection and the merger of individual low-level, mesoscale [O(10 km)] vortices were both important for the simulated genesis of Hurricane Diana (1984). The convectively generated, low-level vortices acted as the building blocks of the simulated hurricane vortex while the toroidal circulation organized the angular momentum associated with the vortices.

The Hendricks et al. (2004) vorticity-based description can be translated to the PV framework using the "PV substance" approach of Haynes and McIntyre (1987, 1990). Within a developing tropical storm, isentropes are nearly flat and quasi stationary. As air passes through isentropic surfaces in convective updrafts, the PV substance is left behind according to the impermeability theorem, resulting in an increased concentration of PV substance (i.e., generation of PV) in the lowest isentropic layers. The net toroidal circulation specifies the system-scale rate of PV generation, while the localization and persistence of updrafts determines the extent to which PV is generated within multiple intense, small-scale vortices. Both the toroidal circulation and small-scale vortex interaction and axisymmetrization can serve to concentrate and organize PV into a tropical-storm-scale vortex.

An observational analysis of the formation of Tropical Cyclone Ed (1993) near Guam (Stewart and Lyons 1996) supports the idea that small-scale vortices can merge and act as building blocks for tropical cyclones. Rapid intensification of the cyclone began after the main eye circulation "ingested" a series of thunderstorms with mesocyclones. Multiple mesoscale vortices are also frequently noted by the Tropical Prediction Center (TPC). Published examples of such vortices in the Atlantic include Isabel (1985) (Stossmeister and Barnes 1992) and Gustav (2002) (Hendricks et al. 2004).

Although convective- and larger-scale PV superposition has not previously been documented to occur simultaneously within tropical cyclones, there is no known dynamical barrier to such superposition. For example, the disturbance that preceded Hurricane Diana originally deepened as a moist baroclinic cyclone when an upper-level PV anomaly approached a stationary

surface front (Davis and Bosart 2001). By increasing the low-level vorticity, the modest baroclinic strengthening had an effect similar to that expected when two large-scale PV anomalies vertically superpose. The upper-level PV anomaly also helped to focus convection along the front near the low-level vortex. In the Hendricks et al. (2004) study, the enhanced low-level vorticity primed the environment for the development of the small-scale vortices within the vigorous convection. These factors were crucial for the rapid development of a stronger surface PV anomaly.

This paradigm will be used herein to investigate the genesis of Tropical Storm Allison, which made landfall along the upper Texas coast in June 2001. The storm is an excellent candidate for such a study because its formation occurred completely within range of the KHGX (Houston/Galveston National Weather Service Office) Weather Surveillance Radar-1988 Doppler (WSR-88D; located at 29.47°N, 95.08°W) and because the storm made landfall within a dense surface observation network.

Information about the synoptic background associated with Allison and a general description of the storm itself can be found in section 2 of this paper. In section 3, details are given on observational evidence for multiple vortices and vortex superposition within Allison. Section 4 contains a discussion of various issues related to mesoscale vortices in tropical cyclones, and concluding remarks can be found in section 5.

2. Synoptic background and system evolution

The environment in which Allison developed was undergoing steady destabilization from synoptic-scale processes. Figure 1 shows the low- and upper-level wind and PV evolution during this time. The low-level return flow on the west side of an East Coast anticyclone had pushed a tropical air mass into south Texas, significantly deepening the low-level moisture. At 0000 UTC 4 June, the Brownsville, Texas, sounding (Fig. 2c) indicated moderate levels (-146 J kg^{-1}) of convective inhibition (CIN), high levels (2272 J kg^{-1}) of convective available potential energy (CAPE), and a moist layer extending to roughly 900 hPa. By 0000 UTC 5 June (Fig. 2d) the CAPE had increased slightly, the CIN had disappeared, and the moist layer had deepened to 750 hPa. Although the CAPE in the Corpus Christi, Texas, sounding decreased somewhat from 4 to 5 June (see Figs. 2a,b), the increase in low-level moisture and disappearance of CIN positively influenced the potential for convection. The approach of a weak upper-level trough and its associated PV (Fig. 1) resulted in synoptic-scale ascent and further destabilization over the northwestern Gulf of Mexico.

Allison quickly developed in the northwest Gulf amidst a series of MCSs (labeled 2 and 3 in Fig. 3) that formed along a north–south line near the upper-level trough axis on the evening of 4 June. The first convective burst associated with what would become a primary low-level vortex began around 0800 UTC 5 June (circle A in Fig. 3). Reflectivity data from KHGX clearly showed a mesoscale vortex embedded within deep convection as early as 1100 UTC (not shown). Reconnaissance aircraft arrived near 1900 UTC, and the flight-level observations allowed the airborne observers to estimate 25 m s^{-1} surface winds and a 1004-hPa surface low. At that point the system was declared a tropical storm by the TPC.

Allison's wind and precipitation distributions were highly asymmetric. Most of the precipitation associated with the storm remained on the east and north sides of the circulation, which was approximately downshear of the storm-scale circulation. This distribution of convection relative to a tropical cyclone circulation in the presence of vertical wind shear is common (Corbosiero and Molinari 2002). Meanwhile, the surface anticyclone to the east of Allison contributed to a substantial pressure gradient over the central Gulf of Mexico, and multiple oil platforms and ships reported tropical storm force winds (i.e., greater than 17 m s^{-1}) hundreds of kilometers from the center of circulation. The highest sustained surface winds measured along the coast during the duration of the storm were only about 15–20 m s^{-1}. Surface wind speeds on the west side of the circulation were generally less than 10 m s^{-1}.

A broad, low-level circulation and multiple circulation centers made tracking the system difficult. According to TPC advisories issued in real time, Allison did not make landfall until after 0400 UTC on 6 June near Galveston, Texas. The best-track postanalysis issued by the same agency shows the storm making landfall before 0000 UTC on 6 June.

Mesoscale analyses of Allison during her landfall reveal the development of an interesting low-level, frontlike structure with the system in the absence of any synoptic-scale baroclinic zone. During the hours before the storm made landfall, a substantial cold pool associated with precipitation that preceded Allison's landfall formed just inland over southeast Texas. Mesoscale analyses (Fig. 4) show the development of surface temperature differences of about 4°C as the circulation began to interact with the cold pool. The structure quickly evolved into something reminiscent of an occluded midlatitude cyclone, with the surface low connected to the frontlike features by a pressure trough. The limited amount of surface data available over the interior of

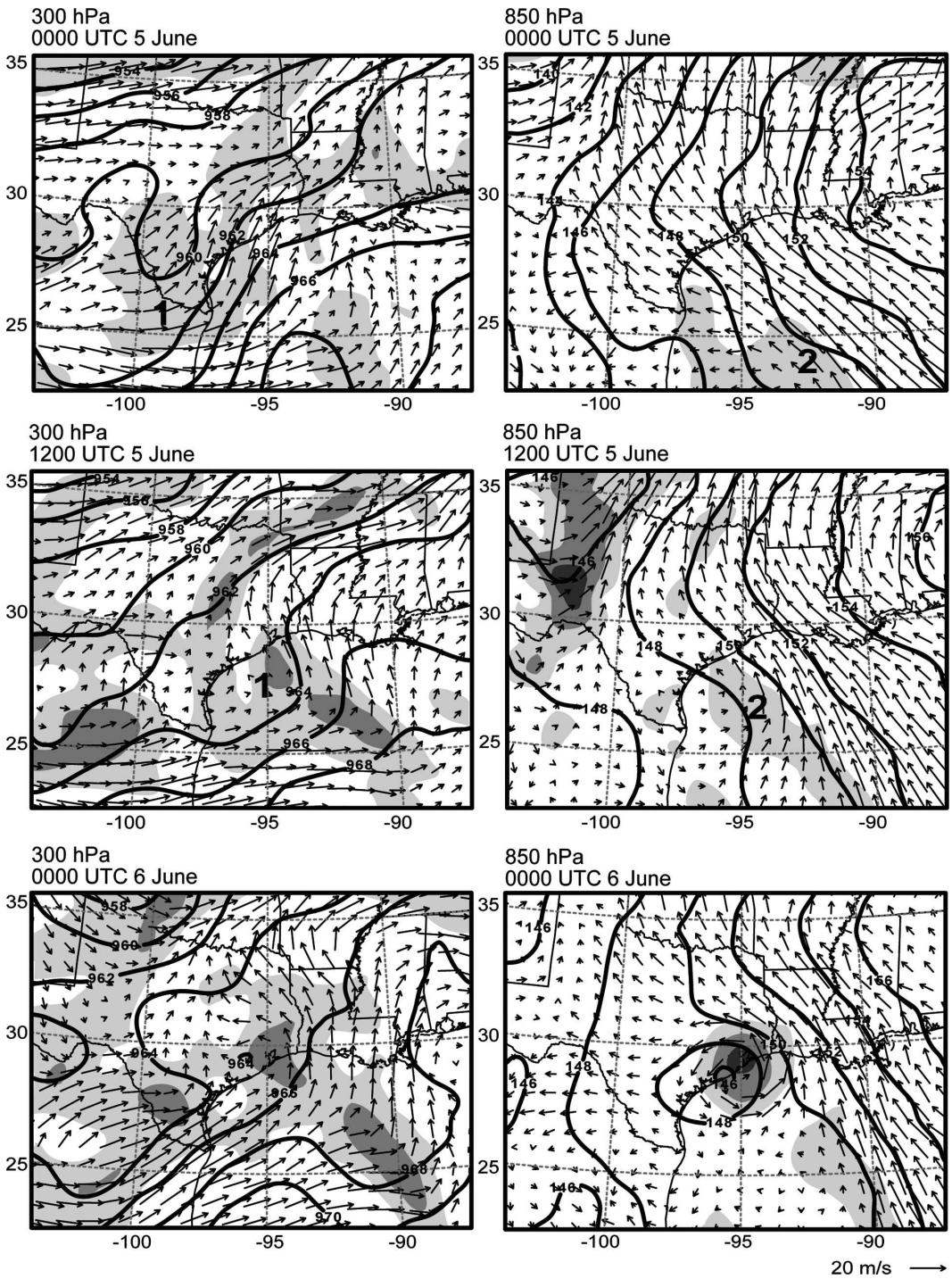

FIG. 1. Eta analyses of 300- and 850-hPa heights, winds, and PV for 0000 UTC 5 June, 1200 UTC 5 June, and 0000 UTC 6 June. Heights are contoured with bold black lines in 20-dm increments, winds are given with arrows (see representative vector in lower right corner), and PV is shaded in 0.5-PV unit (PVU) increments, starting at 0.5 PVU (1 PVU = 1.0×10^6 m^2 K kg^{-1} s^{-1}). The bold 1 is used to indicate the upper-level trough mentioned in text, and the bold 2 is used to indicate low-level PV anomaly mentioned in text.

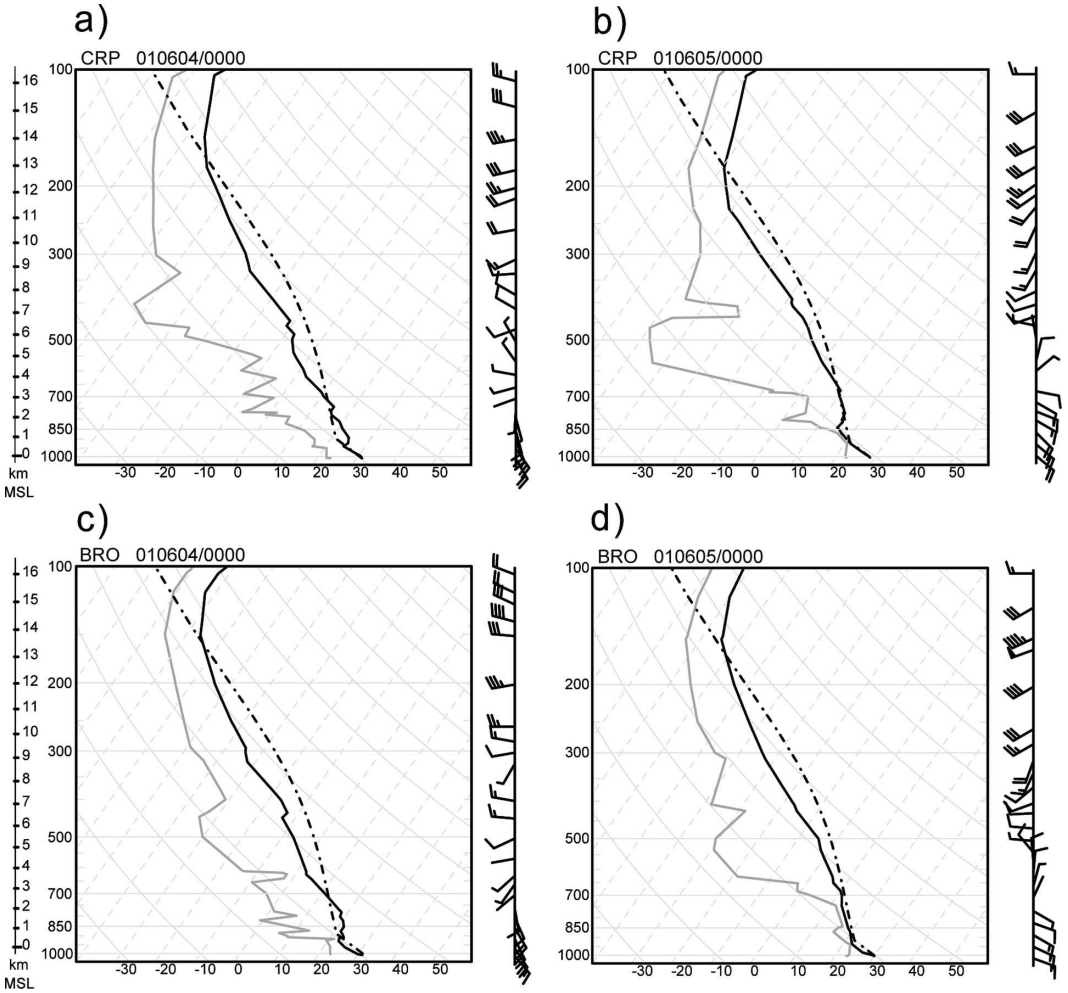

FIG. 2. Soundings from Corpus Christi (CRP) and Brownsville (BRO) from (a), (c) 0000 UTC 4 June and (b), (d) 5 June. Dewpoint is shaded light gray, temperature is in dark gray, and the lifted surface-based parcel trajectory is in black dash–dot.

eastern Texas indicates that the frontlike structure remained through at least 1200 UTC 6 June.

Figure 4 also shows the evolution of the precipitation structure around and just after the time of landfall. All convective precipitation near the center gradually vanished as a rainband just east of the leading edge of the cold pool became the focus for convection. Meanwhile, a large area of stratiform precipitation formed north of the effective warm front. This structure was also reminiscent of a midlatitude cyclone, although the primary rainband was 25 km ahead of the surface "cold front."

3. Multiscale vortices

The remainder of this paper discusses features on various horizontal scales as defined by Orlanski (1975). The scales refer to the following ranges of length: syn-

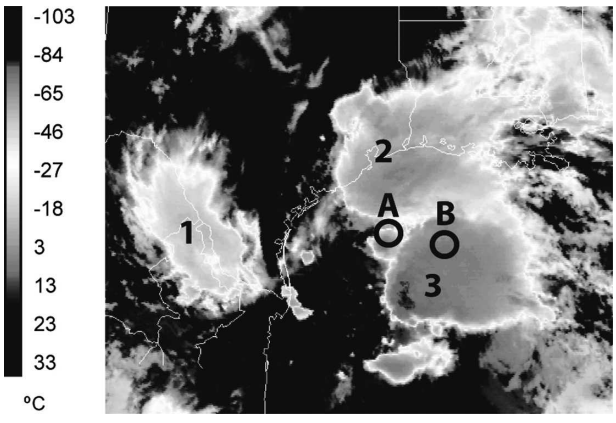

FIG. 3. *GOES-8* IR image of Allison's initial convective burst and ongoing MCSs at 0845 UTC 5 June. Each number represents a distinct MCS, and the two bold circles denote the two convective areas in which vortices A and B developed.

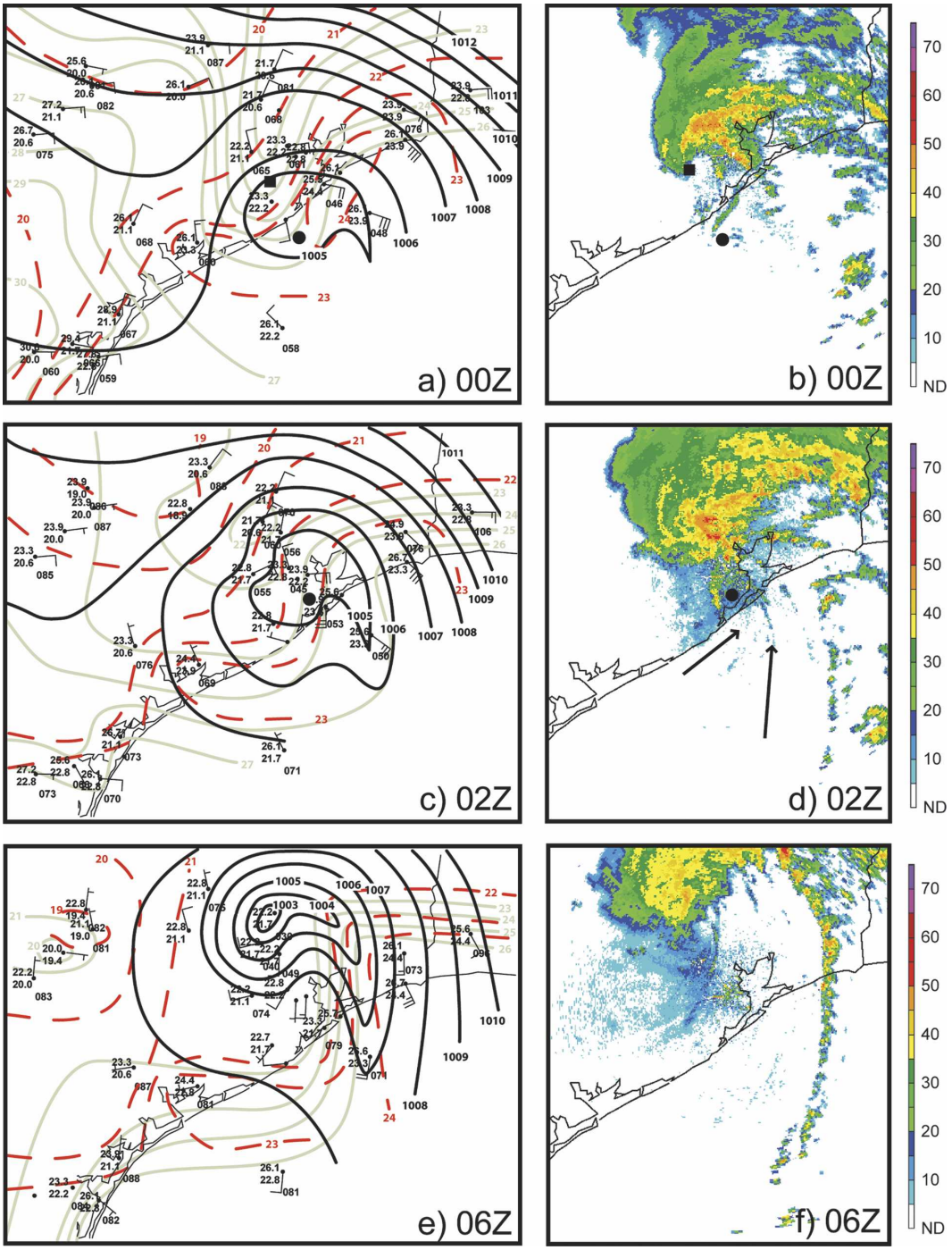

FIG. 4. Mesoscale surface analyses and KHGX radar images from (a), (b) 0000, (c), (d) 0200, and (e), (f) 0600 UTC 6 June. Full wind barbs are 5 m s^{-1} and analyzed fields are as follows: pressure (thick black lines) contoured every 1 hPa, temperature (thick green lines), and dewpoint (thick red dashed lines) contoured every 1°C. The arrow in (d) denotes minor banding around vortex B. The black circles in (a)–(d) denote vortex B, and the black square in (a) and (b) represents vortex C. Scale on right is in dB*Z*.

optic (1000–10 000 km), meso-α (100–1000 km), meso-β (10–100 km), meso-γ (1–10 km), and microscale (<1 km).

a. Methods for determining scale and strength

The scale of any vortex discussed in this study is defined as twice the radius of maximum winds (RMW). The RMW of a vortex was generally estimated using radial velocity data. To estimate the RMW, the position of a given vortex was first identified by finding the center of its flow-relative velocity couplet. The radius at which the velocity differential across the couplet was largest was determined to be the RMW. When available, aircraft observations were also used to estimate the RMW. Another measure of vortex size, the outer radius, is the radius at which the couplet became indistinguishable from variations in the background wind field. Rotational velocity is defined as one-half the sum of the maximum inbound and outbound velocities associated with a vortex. The rotational velocities given herein were estimated from visual inspection of 0.3° radial velocity data unless otherwise noted.

The analyses herein utilize radar data that was transformed to a Cartesian grid with a spacing of 0.5 km for radial velocity data and 1.0 km for reflectivity data. The KHGX radar has a nominal beamwidth of 1° and collects data with a gate spacing of 0.25 km for radial velocity data and 1.0 km for reflectivity data. Note that at a distance of 30 km, the width of the radar beam will be about 0.5 km (which is the same spacing used with the Cartesian transform herein), and it will continue to linearly increase with distance.

b. Synoptic and meso-α scales

On the synoptic scale, the analyses from multiple operational models indicated a low-level PV anomaly associated with the low-level jet that was distinctly different from the anomaly at mid- and upper levels. This feature, labeled "2" in the Eta analysis in Fig. 1, moved into the Gulf of Mexico from the southeast. Meanwhile the upper-level trough, labeled "1" in Fig. 1, approached from over Mexico and superposed over the lower anomaly.

Scatterometer-derived surface winds exceeded 10 m s^{-1} over much of the western Gulf of Mexico on 4 June, and this southeasterly flow strengthened with height to a 20 m s^{-1} 850-hPa low-level jet (Fig. 1). With the presence of an upper-level trough, the southwesterlies at 300 hPa were 10 m s^{-1} over the western Gulf and over 20 m s^{-1} along the Texas coast (Fig. 1). Thus, 200–850-hPa zonal wind shear over the entire western Gulf (Fig. 5) was far greater than the 12.5 m s^{-1} value cited by DeMaria et al. (2001) as unfavorable for tropical cyclone development.

During 5 June, the superposition of the upper and lower PV anomalies favorably altered the synoptic-scale environment for tropical cyclogenesis. By 1200 UTC 5 June, the two PV anomalies had become vertically stacked and winds associated with the two PV anomalies were in a consistent direction throughout the troposphere. Not only did this bring the vertical wind shear down to a favorable value (Fig. 5), but the strengthened surface winds would have enhanced the surface fluxes of latent and sensible heat.

The meso-α-scale generation of PV was also important in Allison. The Eta analysis in Fig. 1 shows a 0.5–1.0 PVU increase in PV and concomitant formation of a closed meso-α-scale circulation at 850 hPa between 1200 UTC 5 June and 0000 UTC 6 June. The only available source for this low-level PV was the widespread deep convection present with the developing tropical cyclone. Thus, the system-scale convective generation of PV helped to establish Allison's meso-α-scale circulation.

c. Meso-β-scale vortices

Meso-β-scale vortex interaction was also important during the genesis of Tropical Storm Allison. Radar and satellite imagery give convincing evidence for three near-surface, meso-β-scale vortices within this storm. For the purpose of this study, they will be referred to as "A," "B," and "C." The vortices were tracked from their apparent points of origin until after the storm made landfall using a combination of reflectivity loops, visible satellite loops, and Doppler velocity data. The tracks are shown in Fig. 6a.

Vortices A and B came within Doppler velocity range at about 1530 UTC. Both vortices were associated with strong convection, and the localized areas of convection can be traced back at least to 1202 UTC in the radar (Fig. 7; see also the earlier IR satellite image in Fig. 3). In the case of vortex A, reflectivity loops clearly show evidence of early rotation, and Fig. 7 shows a curved band of convection wrapping around the vortex center. Based on reflectivity and IR satellite evidence, the localized convection of A originated around 0800 UTC. The rotation associated with B was not unambiguous in reflectivity loops alone, but the convection associated with B originated near 1030 UTC and the track in Fig. 6 follows the convection until B is detectable with radial velocity data.

Vortex A was trackable in radial velocity data (e.g., Fig. 8) until 2000 UTC, and reflectivity loops showed clear evidence of the vortex until 2100 UTC. Vortex B ceased to be trackable in radial velocity data when it

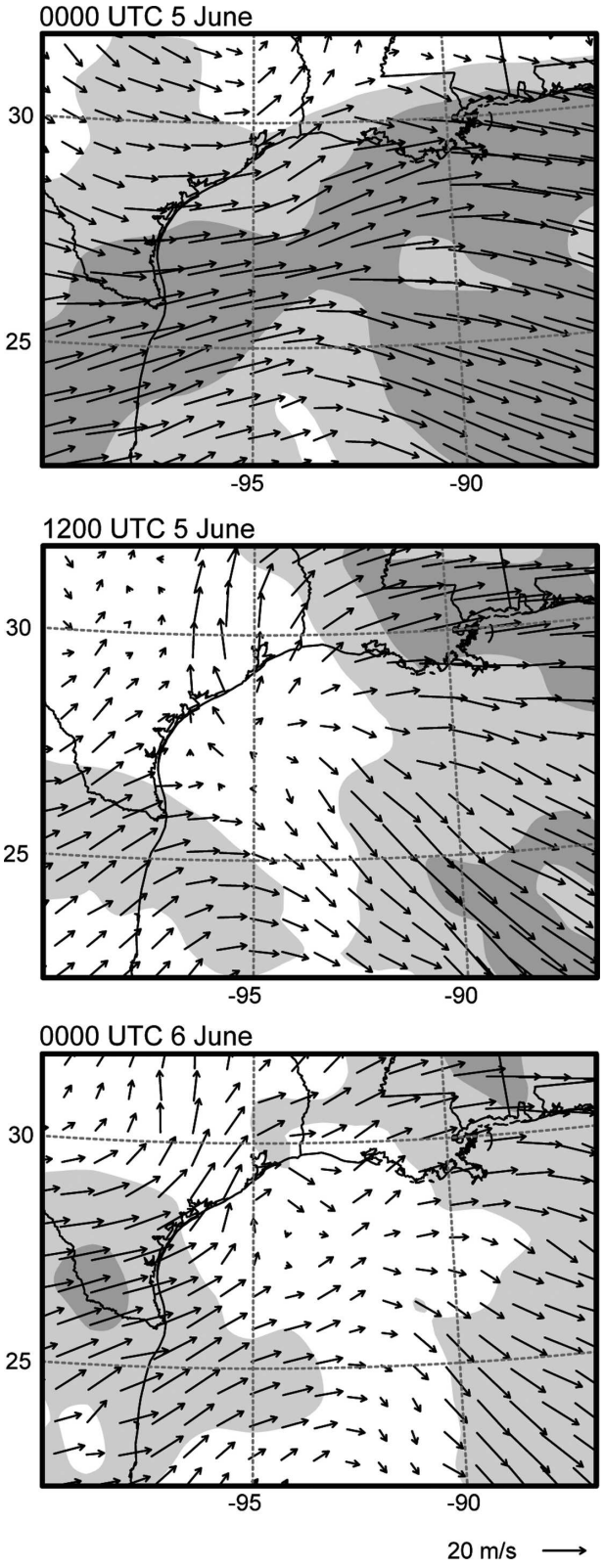

FIG. 5. Eta analyses of 850–200-hPa vertical wind shear for 0000 UTC 5 June, 1200 UTC 5 June, and 0000 UTC 6 June. The magnitude of the shear is shaded with light gray representing 12.5 m s^{-1} and dark gray representing 25 m s^{-1}. Representative shear vector is in lower-right corner.

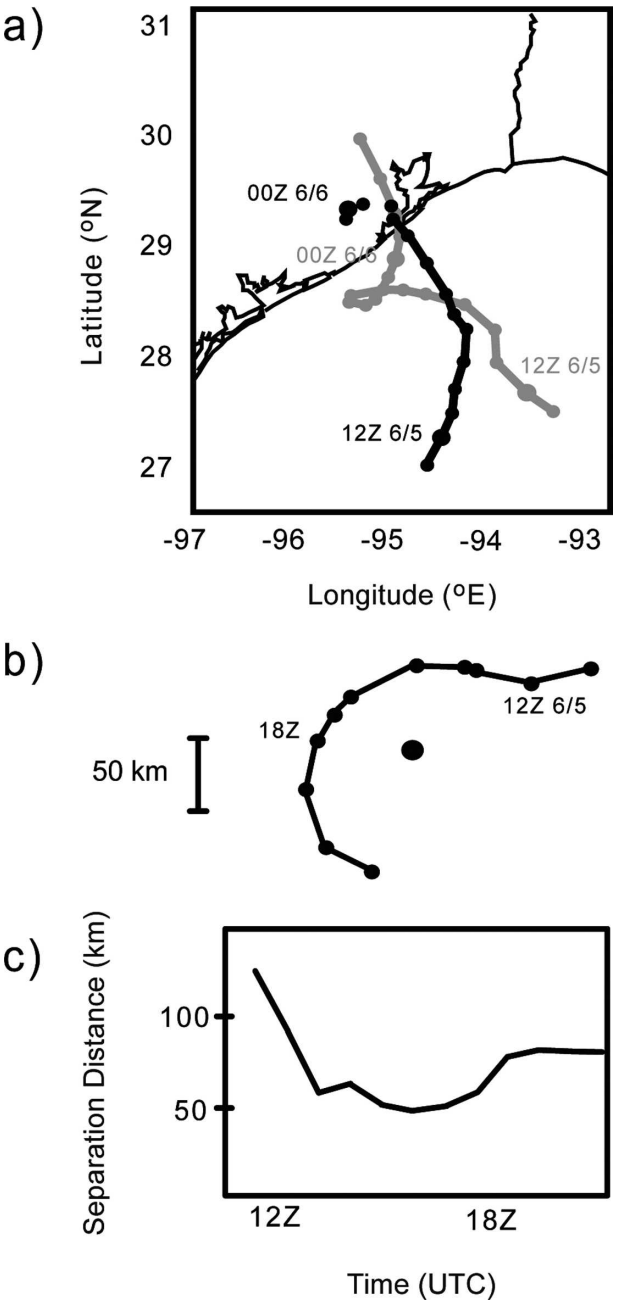

FIG. 6. An analysis of the tracks of the centers of vortices A, B, and C. (a) The tracks of the centers are shown with that of A in black circles connected by lines, B in gray circles connected by lines, and C in black circles not connected by lines. (b) The position of vortex B relative to A is plotted. In both (a) and (b) the individual points mark the location of each center in 1-h time steps. (c) The distance between the centers of A and B is plotted.

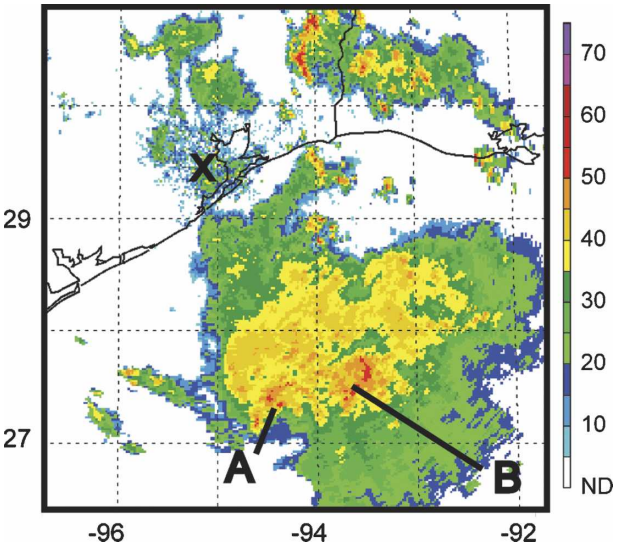

FIG. 7. The 0.3° KHGX radar reflectivity at 1202 UTC 5 June. The locations of circulation centers A and B are indicated and the radar location is denoted with the bold X. Scale on right is in dB*Z*.

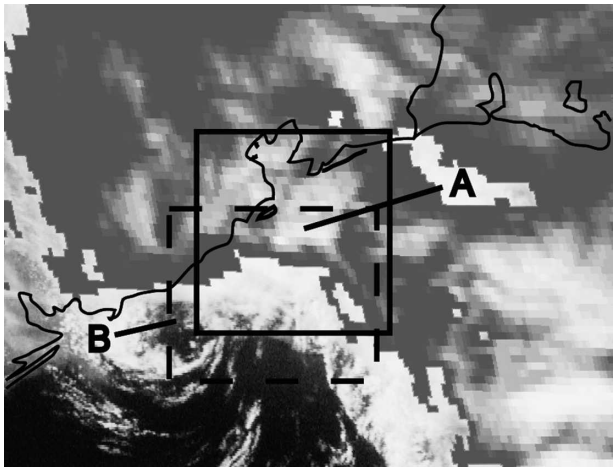

FIG. 9. Overlay of *GOES-8* IR and visible images from 1915 UTC 5 June. The IR overlay starts at temperatures of −30°C and enhancement starts at cloud-top temperatures of about −50°C. The coldest cloud tops in this image are about −65°C. The solid black box denotes the area covered in Fig. 8 while the dashed black box denotes the area covered in Fig. 10. The approximate centers of vortices A and B are noted.

became convectively inactive, but as the cirrus shield moved away from the vortex it was trackable with visible satellite imagery (e.g., Fig. 9) and loops. The cloud swirls associated with B were trackable in visible imagery until sunset (0100 UTC 6 June) and in reflectivity until 0400 UTC. The lowest pressure, accompanied by a closed circulation, was observed at coastal stations at the approximate time where B was inferred to have made landfall (Fig. 4).

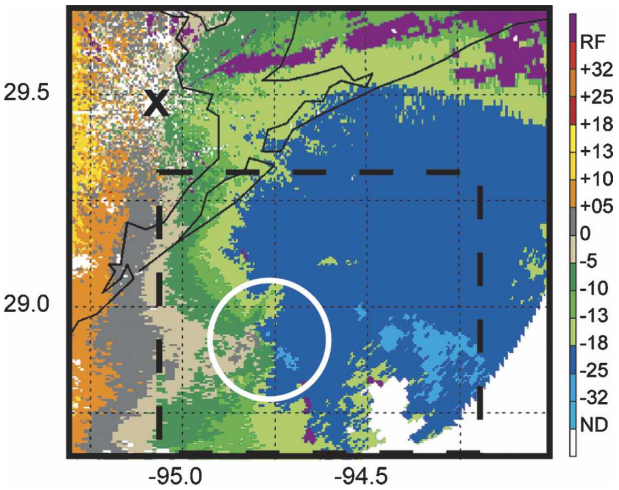

FIG. 8. The 0.3° KGHX radial velocity at 1913 UTC 5 June. Scale on right is in m s^{-1}. Approximate center of vortex A is located at the center of the white circle, and the circle radius is approximately twice the RMW of A. The dashed line represents the domain in Fig. 13. The radar location is denoted with a bold X.

To confirm the existence of vortices inferred from the radar and satellite evidence, an analysis of wind structure at 250 m (Fig. 10) was created from in situ 30-s flight-level reconnaissance observations supplemented with KHGX radial velocity data from the 0.3° elevation angle scan. The radial velocity data was used to estimate wind vectors north and west of 28.8°N, 94.7°W in Fig. 10; this includes a symmetric vortex assumed around A and vectors north and west of that location. The radial velocity data was within 300 m of the altitude of the reconnaissance plane, and the two sources of data were in good agreement where they were horizontally collocated, so the radial velocities utilized were assumed to be valid at the flight level (~250 m). Elsewhere, wind fields were interpolated from aircraft observations (including data not shown near 28.0°N and east of 94.0°W) wherever such observations fit a consistent overall pattern. The use of radar data from a different altitude and reconnaissance data from more than 10 km away introduces significant uncertainty into some areas of Fig. 10, and the subjectively estimated uncertainty is represented by differential shading of the velocity vectors in Fig. 10.

The radial velocity data proved useful for analyzing vortex A because it was poorly sampled by the reconnaissance aircraft. On the other hand, the relative abundance of reconnaissance observations within B compensated for poor sampling of that vortex by the radar. The nominal time of the analysis in Fig. 10 is about 1915 UTC and it approximates the wind field at 250 m. The

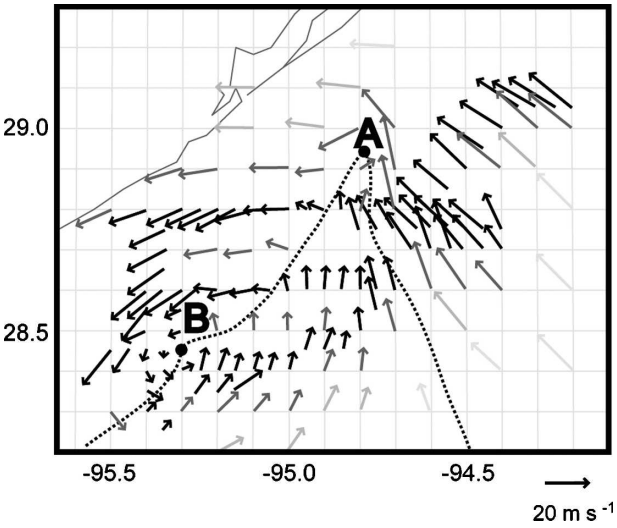

FIG. 10. Flight-level (~250 m) wind analysis. The data utilized are high-resolution reconnaissance observations and KHGX radial velocity, and the nominal time is 1915 UTC 5 June. Arrows are shaded according to subjective certainty. The black arrows represent in situ data obtained from the aircraft. The dark gray arrows represent an estimate of direction taken from the nearest aircraft observation(s) except that a symmetric vortex was assumed for the dark gray arrows around vortex A. The wind speed was obtained by dividing the radial velocity by cosine of the angle between the wind vector and a vector pointing directly at the radar. Uncertainty is highest at locations of light gray arrows, where no reconnaissance observations were available within 25 km. The dashed lines represent the positions of the wind shift line (southwest of A) and the surge line (south-southeast of A). Vortices A and B are labeled.

reconnaissance observations shown were taken between 1810 and 1940 UTC. Vortex B was nearly stationary during this time, so this analysis is approximately equivalent to a reference frame moving with the center of B. Vortex A was moving northeastward at about 8 m s^{-1} during this period but most observations near vortex A were taken within a few minutes of the nominal analysis time. Note that Fig. 10 only gives a snapshot of these vortices at one particular time and is not necessarily representative of the wind field hours earlier or later.

Figure 10 reveals a complex mesoscale wind pattern associated with Allison that is reminiscent of the wind field observed during the genesis of Hurricane Dolly (Reasor et al. 2005). A wind shift line and a surge line terminate at or near the center of vortex A. The wind shift extends southwestward through B, and the surge line extends southeastward. The wind direction shifted about 60° over 5 km along the wind shift while the change in wind across the other line was mostly in strength, fitting the definition of a surge line. The winds south and west of the two lines (generally between the two vortices) were much weaker than those north and east of the lines.

Vortex B appears to be the dominant vortex, while A barely has a closed circulation. This distinction is solely a kinematic consequence of the different translation velocities of the two vortices. When wind vectors are reduced to a frame of reference moving with A (not shown), A takes on the appearance of the dominant vortex and B's circulation is barely closed. Thus, there was no single, dominant vortex within Allison at this time.

A possibly more significant difference between the two vortices at the time of the analysis in Fig. 10 was with respect to the RMW. At the analysis time, the RMW of A (though multiple elevation scans) was about 6.5 km, while that of B was about 15 km. These differences may be the result of differences in convection between the two vortices; B was convectively inactive and A was associated with a large area of vigorous convection. The convection in A may have caused a deep inflow layer that concentrated its vorticity into a relatively small area.

Vortex C formed at around 2200 UTC from within a 20–30-km-wide area of intensifying deep convection (see Fig. 11). The vortex tracked cyclonically around the area where A was last tracked, and its path did not take it close to the surface observations.

The convective structure of C quickly changed after it formed. Although the vortex developed within an area of deep convection, the precipitation over the center of C rapidly weakened. In its place, a large band of 45–60-dBZ precipitation encircled more than 50% of the vortex near its RMW. Figure 12 shows a close-up view of 0.3° reflectivity and radial velocity data at 2219 UTC.

This evolution is markedly similar to that observed during the formation of the eye of Tropical Cyclone Ed early during its genesis phase (Stewart and Lyons 1996). The authors of that study hypothesized that a rapid increase in the low-level wind field about a small meso-β-scale vortex was the result of a large convective burst within the tropical depression. They further hypothesized that the wind field quickly became supergradient and induced subsidence within the RMW. The convection near the vortex center quickly died while a band of precipitation encircled the vortex near the RMW, forming the eye of what would eventually become Ed. Although this nascent eyewall was only composed of 25–35-dBZ convection, Stewart and Lyons (1996) report that this vortex remained the eye even as Ed strengthened to supertyphoon strength.

As vortex C continued to move inland, it became more disorganized. By 2300 UTC the vortex had be-

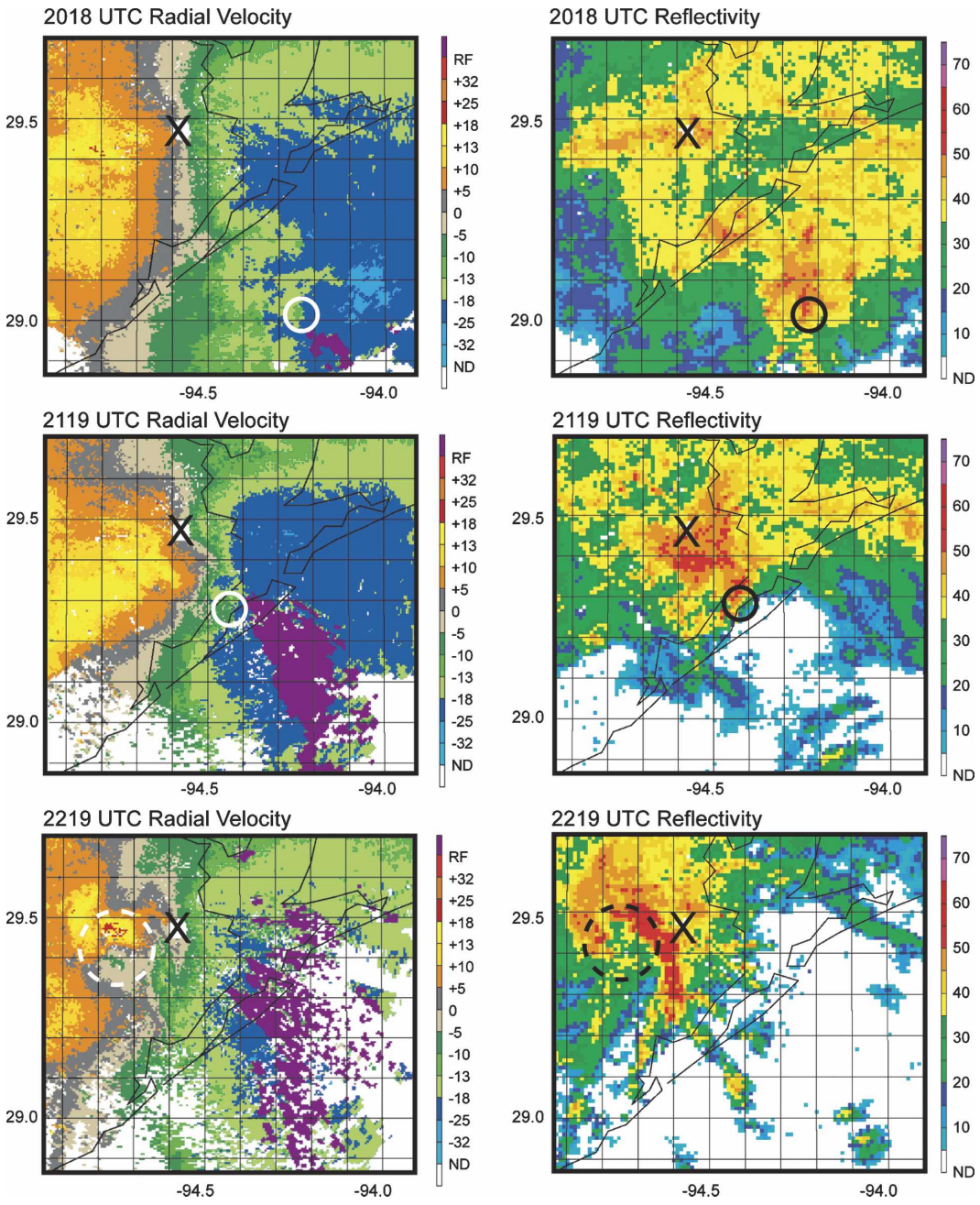

FIG. 11. Meso-γ vortex C1 at 2018 and 2119 UTC and meso-β vortex C at 2219 UTC in 0.3° KHGX radial velocity and reflectivity data from 5 June. Vortex C1 is located at the center of the solid circles and vortex C is located at the center of the dashed circles. The circle radius is approximately twice the associated vortex RMW. The radar location is denoted with a bold X. The velocity scale is in m s^{-1}, and the reflectivity scale is in dBZ.

come somewhat separated from the deep convection as it moved farther west. At this time, the vortex was only surrounded about 30% by 30-dBZ convection. It was also at this time that the rotational velocity reached a peak of 30 m s^{-1} within the lowest kilometer above the surface. Thereafter, the low-level vortex began to rapidly weaken, and it was difficult to follow by 0100 UTC in the lowest 1 km of radial velocity data. The vortex weakened slower at slightly higher levels and was trackable in the 2.3° radial velocity data (about 3 km) until about 0130 UTC. After this time, its circulation was too weak to distinguish from the background flow, and only hints of elevated vorticity remained in the radial velocity data at low levels to the west of the radar.

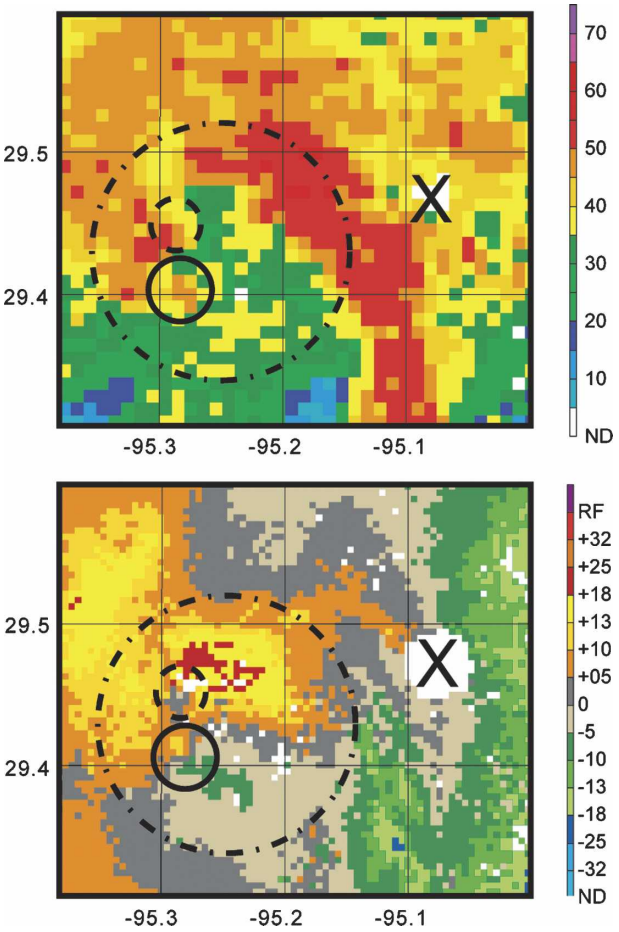

FIG. 12. Vortices at 2219 UTC 5 June. Vortex C2 is at the center of the solid circle, and possible vortex C3 is at the center of the dashed circle. The center of vortex C is at the center of the dot–dash circle. The radius of the circles is approximately twice that of the RMW of the encircled vortex. The radar location is denoted with a bold X. The reflectivity scale is in dBZ and the velocity scale is in m s^{-1}.

The meso-β vortices in Allison tended to be strongest at lower levels when they were accompanied by active convection. When their attendant convection waned, they were stronger at higher altitudes. For example, at around 1700 UTC (not shown) there was a lack of deep convection associated with vortex A. At this time, the strongest circulation noted in radial velocity data with this vortex was between 6 and 7 km above sea level. However, after deep convection became reestablished the structure of the vortex changed such that the strongest circulation was within 1 km of the surface. Vortex C demonstrated similar behavior; its strongest circulation was within the lowest kilometer of the atmosphere during and shortly after its period of active convection. After the convection dissipated, the near-surface circulation weakened, leaving the strongest circulation between 2 and 3 km above the surface.

While Fig. 6 shows that vortices A and B moved cyclonically around one another as in Simpson et al. (1997), it is not clear to what extent this movement was due to advection by winds associated with the larger-scale PV anomalies versus interaction between the meso-β vortices. The observed motion of B relative to A was about 8–10 m s^{-1} at a distance greater than 50 km.

Starting at around 2100 UTC, Doppler velocity data (not shown) reveals the development of a midlevel (~6.5 km) vortex near the edge of the stratiform precipitation on the west side of the storm-scale circulation. This MCV gradually built downward as its circulation center drew near the transition zone between convective and stratiform precipitation on the northwest side of the storm-scale circulation. This vortex strengthened to its maximum intensity at about 0130 UTC, when it had a peak rotational velocity near 40 m s^{-1} at an altitude of approximately 4.5 km. Also, as the MCV strengthened, its RMW shrank from 45 to about 25 km.

When vortex B stopped being trackable at about 0400 UTC, its center had rapidly approached to within 35 km of the MCV center. The mesoscale surface analyses in Fig. 4 reveal the evolution to a more concentrated surface vortex with stronger pressure gradients by 0600 UTC. The lowest surface pressure measured as Allison made landfall was 1004 hPa, but the central pressure later fell to less than 1003 hPa even as deep convection weakened. Note that the central pressure fell in spite of an environmental tendency for pressure rises and resulted in the stronger pressure gradients in Fig. 4c. The surface winds did not intensify when the pressure gradient strengthened, perhaps because of increased surface friction over land and the ongoing dissipation of deep convection near the merged centers.

d. Meso-γ-scale vortices

It became apparent as vortex A neared the KHGX radar that meso-γ-scale vortices associated with individual convective cells were embedded within the meso-β-scale vortex. These vortices, some of which are shown in 0.3° radial velocity and reflectivity images in Fig. 13, existed both in the core of convection near the center and in the primary rainband. The typical outer radius of these vortices was less than 5 km while the radii of their parent convective cells were less than 2.5 km. The vortices tended to be fairly shallow, with the strongest circulation generally observed in the lowest radar elevations at about 1 km above ground level. With one exception discussed below, the highest low-level reflectivity associated with these convective cells was very near or over the low-level vortex center.

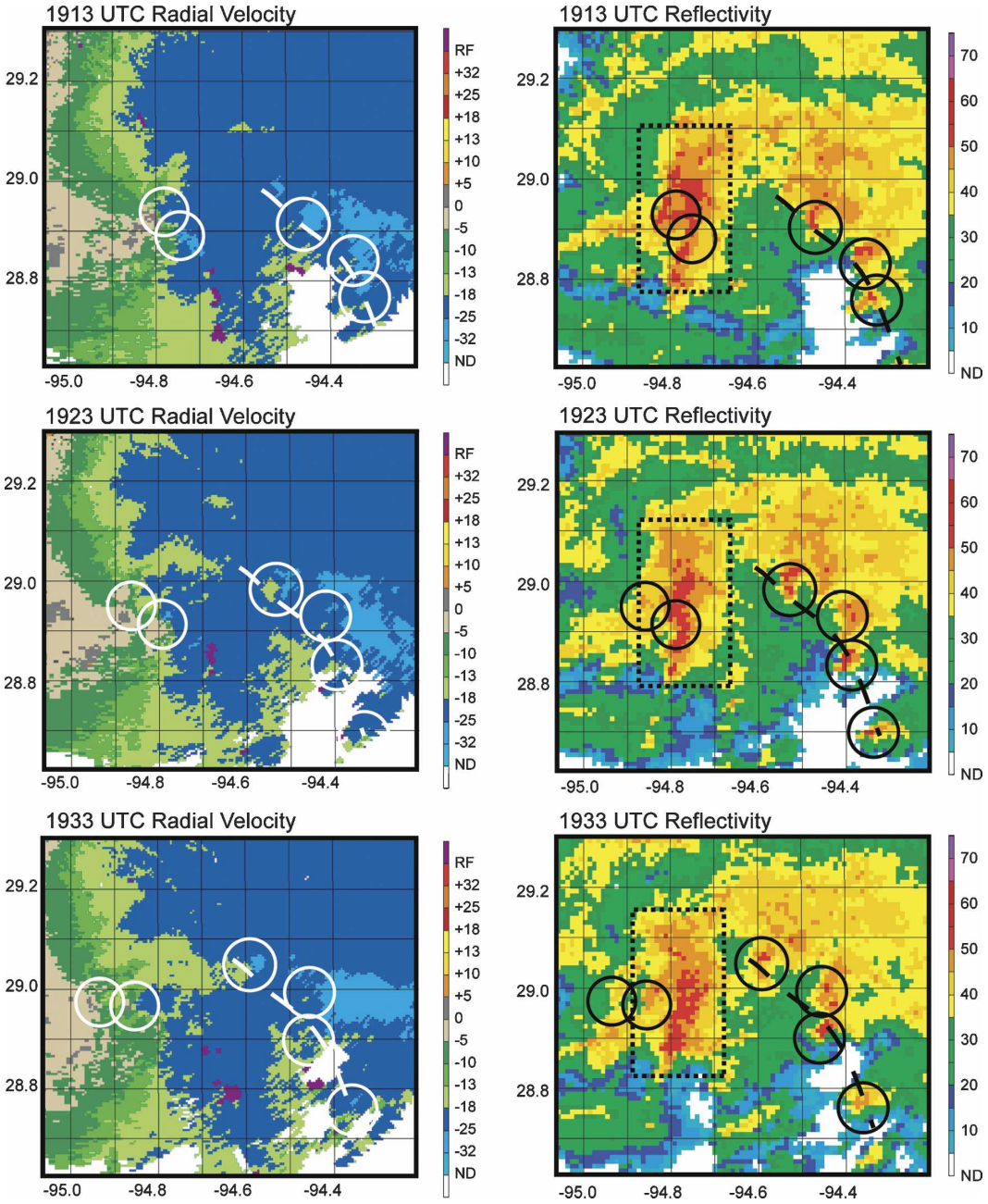

FIG. 13. The 0.3° KHGX radial velocity and reflectivity images from 5 June. For reference, meso-γ-scale vortices discussed in the text are located at the center of the circles. The circle radius is approximately twice the associated vortex radius of the maximum winds. The velocity scale is in m s^{-1}, and the reflectivity scale is in dBZ. The shear/rainband axis is denoted by the white (black) dashed line in velocity (reflectivity) data. Convection enclosed by the dotted line is referred to as "central core convection" in text.

The Doppler-indicated rotational velocity of the strongest meso-γ-scale vortices was as strong as that of a moderate Great Plains mesocyclone. The characteristics of these vortices were also comparable to those of tornadic mesocyclones observed with other Gulf of Mexico tropical systems documented by Spratt et al. (1997). Typical rotational velocities of the previously documented mesocyclones and those observed with Allison generally ranged from 7.5 to 15 m s^{-1}. A typical RMW with Allison's meso-γ-scale vortices was around 2 km, while those investigated by Spratt et al. (1997) ranged from 1 to 1.5 km.

The tracks of all such vortices that were detected as forming between 1830 and 1930 UTC are plotted in Fig. 14 relative to vortex A. Although such features likely existed before this time, they would have been at distances greater than 100 km from the radar. The width and height of the lowest radar beam at such distances would inhibit the detection of such small, shallow vortices. Every plotted vortex formed southeast of meso-β-scale center A and moved cyclonically around it. These vortices tended to have two distinct fates; they either dissipated to the northwest of A or they became ingested into the deep convection east and north of its center.

Allison's meso-γ-scale vortices formed in an environment of locally enhanced vorticity and strong surface winds. Many of the vortices dissipated on the west side of vortex A where weaker surface winds likely resulted in reduced surface fluxes. In addition, the mesocyclones formed within the RMW of vortex A or along a shear axis associated with the primary rainband (see Fig. 13), about 35 km east of the surge line shown in Fig. 10. These were both areas of locally enhanced cyclonic vorticity, where vorticity stretching likely aided in mesocyclone development.

One particularly intense meso-γ-scale vortex (hereafter C1) formed near the southern extent of the central core convection around 2000 UTC. Snapshots of C1 and its environment are shown at 2018 and 2119 UTC in Fig. 11. As with the other vortices of the same scale, C1 was centered inside a convective cell. At 2003 UTC vortex C1 only existed through the 0.3° elevation scan (about 1 km) and had a rotational velocity of about 7 m s^{-1}. The vortex began to intensify as a strongly convergent velocity signature developed in its lowest levels. This convergence began around 2024 UTC and lasted until 2054 UTC. By 2054 UTC the rotational velocity had increased to about 17.5 m s^{-1} within the lowest 2 km, and the depth of C1 had increased to between 4 and 5 km. The RMW of the vortex within the lowest 2 km was consistently between 2 and 4 km.

Shortly after 2100 UTC, the lowest few kilometers of C1 began to be disrupted by the formation of several smaller meso-γ-scale vortices within 5 km of the vortex center. Thereafter, the circulation of C1 gradually weakened at the lowest levels. By 2130 UTC, there was no circulation detectable below about 3 km. The vortex was last tracked at 2158 UTC as it moved to within 10 km of the KHGX radar. If the vortex existed at 3 km after this time, it would have been too high to be detected by the highest elevation scan of the radar.

While the evolution of C1 after 2158 UTC is ambiguous, it might have been important to the development of C. Vortex C formed around 2200 UTC below 3 km within an area of strong cyclonic vorticity just northwest of where C1 was last tracked. Several other vortices on the same scale as C1 were also nearby at this time. Due to the likely close proximity of these vortices to C at the time it developed, they may have provided a ready source of vorticity for C.

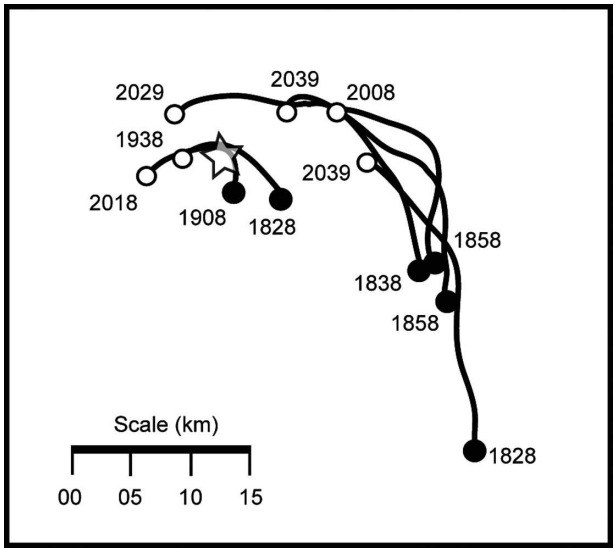

FIG. 14. The tracks of all meso-γ-scale vortices relative to meso-β-scale center A (represented by a star) that formed between 1830 and 1930 UTC 5 June. The filled circles represent points at which the convective cell associated with each vortex attained a precipitation intensity of 50 dB*Z*.

Figure 12 shows at least one meso-γ-scale vortex (hereafter C2) within the wall of deep convection surrounding the center of C during the hour when it was most organized. Vortex C2, while smaller than any other vortex tracked in this study, was the most intense vortex observed. At its peak, it had a rotational velocity of up to 17 m s^{-1} and an RMW of only 1 km. Like the other meso-γ-scale vortices during the event, C2 tended to be associated with a local maximum in reflectivity and rotated counterclockwise around the local meso-β vortex. It formed on the northeast side of C, attained its maximum strength on the west side of the vortex, and dissipated on the southwest side. The vortex evolution was rapid; the time between formation and dissipation was between 20 and 25 min.

There were other possible meso-γ-scale vortices of similar size and strength within the wall of deep convection. However, these features lasted only one to two volume scans, making them difficult to track. One such possible vortex, C3, is suggested by the velocity pattern in Fig. 12. A few minutes later, a report of tornadic wind damage at 29.46°N, 95.34°W was received by the National Weather Service. The possible relationship

between tropical meso-γ vortices and tornadoes merits further investigation.

4. Discussion

a. Mesovortices: Occurrences and importance

On the system scale, a hurricane is an approximately balanced, warm-core vortex with a column of anomalously high PV at its core (Shapiro and Franklin 1995; Willoughby 1990). The formation of such a core, and thus the formation of the hurricane itself, requires the generation of PV within an organized updraft at the appropriate scale and/or the merger of PV anomalies that have been generated at smaller scales. The establishment of a warm-core vortex requires, in particular, the generation of PV at low levels.

With Allison, strong low-level vortices were present at a variety of scales. At the meso-β and meso-γ scales, these vortices existed at least partly within active, deep convection, constraining their lower-tropospheric stratification to be similar to (or slightly higher than) their environment. Because their vorticity was considerably higher than the vorticity of their surroundings, these vortices were certainly positive PV anomalies. Also, because these mesoscale vortices strengthened at low levels during periods of surface-based convection, their low-level PV was being produced by the convection.

The tracking of these vortices shows that superposition of PV anomalies took place at the meso-β scale and might also have occurred from the meso-γ to the meso-β scale (as in Montgomery and Enagonio 1998; Hendricks et al. 2004; Montgomery et al. 2006). For example, on the meso-β scale, a midlevel MCV appeared to merge with vortex B. The result was a more clearly defined surface center in both the pressure and wind fields. On the meso-γ scale, it is difficult to say to what extent vortex merger was relevant in the Allison case. While the convection north and east of meso-β center A did ingest multiple meso-γ vortices, this did not appear to have any effect on the storm structure. Yet, several meso-γ vortices were present in the vicinity of where vortex C quickly formed. The presence of such vortices presents the interesting possibility of meso-γ merger helping to build a larger vortex. The convection associated with the meso-γ vortices was also an important source of PV production within the larger-scale vortex.

Because of the limited number of case studies focusing on the mesoscale details of tropical cyclogenesis, it is difficult to say exactly what role multiple meso-β- and meso-γ- scale vortices play during tropical cyclone development. To our knowledge, observations of multiple meso-β-scale vortices other than MCVs have only been documented in refereed literature by Stossmeister and Barnes (1992), Hendricks et al. (2004), Reasor et al. (2005), and the present study. Furthermore, observations of multiple meso-γ-scale vortices in a developing tropical cyclone have only been previously discussed by Stewart and Lyons (1996). Despite the relative absence of observations of these smaller-scale vortices in studies relevant to tropical cyclone formation, the existence of rainband and eyewall meso-γ-scale vortices in mature tropical cyclones has been extensively documented (e.g., Spratt et al. 1997). Also, the frequent mention of meso-β-scale vortices in TPC forecast discussions indicates that they too are fairly common.

The small scales of these vortices make them exceptionally difficult to observe in many cases. Convectively active meso-β-scale vortices can only be remotely detected by Doppler radar, and satellites can detect such vortices only if their convection dissipates and the low-level cloud swirl becomes exposed. It is for this reason that sheared environments result in the most easily observable meso-β-scale vortices when storms are far from shore. Most reconnaissance flights are on a mission to find a single center of circulation and may not be able to fully investigate others. Meanwhile, meso-γ-scale vortices are likely to go unobserved with in situ airplane observations and can only be reliably observed with horizontally scanning Doppler radar.

b. Tracking issues

The occurrence of multiple meso-β-scale vortices presents a difficulty in tracking developing tropical cyclones. In the 2003 season alone, the presence of such features complicated TPC tracking of at least four Gulf of Mexico tropical systems (Bill, Claudette, Henri, and Grace). One particular TPC forecast discussion for Claudette indicated that the feature being tracked as the center appeared to be rotating around a broader circulation. Furthermore, TPC discussions often speak of the center of circulation jumping from one convective flare-up to another, with multiple candidates for the true circulation center. This often happens in high-shear cases when convection gets displaced downshear of a circulation center (e.g., Molinari et al. 2004), resulting in pressure falls and center regeneration under the convection. The fates of these circulation centers vary and include merger, dissipation, and hurricane genesis (Stewart and Lyons 1996; Reasor et al. 2005).

Pinpointing an arbitrary single center of a multiple-vortex tropical cyclone becomes a particular concern when such a system nears land. Tracking a single vortex as the center can mean the landfall of another vortex and its associated weather hundreds of kilometers from

where the official center is being tracked. In the case of Allison, convection-free vortex B was tracked as the official center as C and its associated convection moved over the suburbs of Houston. Similar events happened with tropical storms Fay (in 2002) and Grace (in 2003), both of which made landfall near the upper Texas coast. As was the case with Allison, tropical storm–force winds and major flooding might accompany these other well-defined centers, while mostly clear skies and light winds might accompany the official center.

c. Tropical vortices and MCVs

Although the terms "tropical storm" and "tropical depression" are convenient for operational use, some systems so labeled may be dynamically indistinguishable from many convective systems over land. A closed surface circulation associated with organized deep convection is called a tropical depression in some contexts, but the same sort of system can develop over land when new convection forms beneath old MCVs (e.g., Rogers and Fritsch 2001). There is also a continuum in the PV framework between an MCV and a weak tropical cyclone consisting of vortices with maximum winds at various levels. In some cases, the only kinematic justification for distinguishing systems with surface circulations over water from their counterparts over land is their potential to develop into hurricanes through the separate dynamical mechanisms of mesoscale vortex merger (e.g., Hendricks et al. 2004) and WISHE (see also Montgomery et al. 2006).

d. Vortical hot towers and convective burst vortices

While the meso-β-scale convective vortices in Allison appear similar in strength and size to the "vortical hot towers" (VHTs) simulated and discussed by Hendricks et al. (2004) and Montgomery et al. (2006), it is difficult to say how the observed meso-β-scale vortices actually relate to VHTs. The structure and scale (15–30 km) of the reflectivity pattern associated with A imply a complex of individual updrafts. These updrafts stimulated significant asymmetries in the circulation of A on a scale that the aforementioned numerical simulations could not have resolved. Under the assumption that the smallest resolvable features in a numerical simulation are 5 times the grid spacing, the 15-km-wide VHTs in these numerical studies were the smallest structures that could be resolved by Hendricks et al. (2004). Their investigation noted that finer-resolution numerical simulations tended to produce smaller VHTs than those with a 2- or 3-km grid spacing. Also, unlike the meso-β vortices in Allison, the simulated VHTs tended to be symmetric. Thus, the modeled vortices may be dynamically akin to Allison's meso-γ-scale vortices, but simulated at the model's smallest resolvable scale.

The intrinsic scale of a hot tower does not seem to have been formally defined in peer-reviewed literature, but the term has historically referred to individual cumulonimbi with approximately 5-km-wide updrafts (e.g., Reihl and Malkus 1958; Malkus et al. 1961; Simpson et al. 1998). As indicated above, the structure and scale of the deep convection associated with A imply a complex of individual updrafts rather than a single hot tower. Instead, the hot towers of Allison were likely the convective cells associated with the meso-γ-scale vortices.

If the meso-β vortices were not vortical hot towers, what were they? While at least one meso-β vortex was an MCV, others were not. Meso-β vortex C formed rapidly within a mass of intense convective cells and was thus distinguishable from a typical MCV in formation mechanism (i.e., active convection versus stratiform/melting level) as well as horizontal and vertical structure (i.e., smaller and at lower levels). Although the evidence is less conclusive, vortices A and B also appeared to form within bursts of convection on scales larger than an individual cell. To distinguish these particular meso-β vortices from MCVs and VHTs, we dub them "convective burst vortices," or CBVs.

5. Conclusions

This article has explored the extent to which the processes of PV generation and superposition were relevant across many scales of motion during the genesis of Tropical Storm Allison. While further analysis is necessary to better understand some aspects of the meso-β- and meso-γ- scale evolution, it is clear in this case that multiple-vortex formation was a key component of cyclogenesis through several scales. While only the case of Allison has been discussed in great detail, other studies have documented PV superposition on various scales. In addition, multiple mesoscale vortices are often apparent in many developing tropical cyclones.

With multiple vortices (at multiple scales) possibly participating in tropical cyclogenesis, a single mode of development may not exist. For example, while Montgomery et al. (2006) simulated the development of a tropical cyclone with just *one* initial MCV, other cases (e.g., Ritchie and Holland 1997) have seemingly required the merger of multiple MCVs to adequately prime the environment for cyclogenesis. Potential vorticity superposition on larger scales may be required so that low-level PV "building blocks" can even form in some cases. With Allison, for example, meso-β-scale convective burst vortices developed very quickly within

areas of deep convection *after* larger-scale PV superposition created an environment where increased instability, enhanced surface fluxes, and elevated low-level PV coexisted. Ultimately, for WISHE to initiate, it may not matter what type and combination of vortices are present, as long as adequate surface wind speeds and system organization are present.

While we do not know whether surface winds crossed the WISHE threshold in this instance, Allison does illustrate that strong surface winds can be present due to preexisting and interacting synoptic- and meso-α-scale features before a closed surface low forms. If those winds are tropical storm force, a closed warm-core vortex instantly becomes a tropical storm according to operational definitions, bypassing the tropical depression stage altogether. This presents the interesting possibility that incipient tropical cyclones that form in strong low-level flow do not initially induce much oceanic heat flux from their own circulations. Instead, preexisting strong winds and enhanced surface fluxes might conceivably "jump-start" WISHE and lead to rapid hurricane development in some instances. Such enhanced fluxes may also have played a role in the propensity of low-level vortices to develop and intensify within Allison.

While convective burst vortices and downward-developing MCVs are of great interest for understanding tropical cyclogenesis, they also present considerable forecasting implications. A significant forecasting problem lies in the paradigm that, given a tropical cyclone, an exact center of circulation must exist. Although this idea works well for well-developed systems, such as a hurricane with an eye, it is inappropriate for a developing tropical storm. Rather, the tendency is for many developing systems to be composed of a diffuse area of elevated PV with small, concentrated areas of particularly high PV.

Although Tropical Storm Allison provides an interesting glimpse into rarely documented mesoscale processes in tropical cyclogenesis, many of the observations and conclusions drawn herein are subject to the limitation of coming from a single case. For example, the importance of the documented meso-γ-scale vortices to tropical cyclogenesis in general remains unknown. Few published observational studies have focused on meso-β or meso-γ scales. Although this is at least partly due to a lack of data over the ocean, the occurrence of landfalling tropical cyclones in their development stage is common enough that other similar studies are possible. Detailed analyses of other cases should address much of this uncertainty and provide for a more complete understanding of tropical cyclone formation.

Acknowledgments. Aircraft reconnaissance data were provided by James Franklin of the Tropical Prediction Center. Discussions with Michael Montgomery were helpful for understanding the nature and possible ubiquity of vortex interaction and merger. Christopher Davis and an anonymous reviewer helped to clarify and improve this manuscript. Portions of this work were supported by the National Oceanic and Atmospheric Administration through Award NA17WA1011.

APPENDIX

Potential Vorticity: Nomenclature and Concepts

The purpose of this appendix is to describe the basic concepts and nomenclature of potential vorticity (PV) as applied in this paper. While the use of PV has gained favor in the research community, it remains a somewhat unknown quantity in much of the operational community.

Potential vorticity can be expressed in various forms. Here it is sufficient to consider the Rossby form of PV, expressed as the isentropic layer mean vorticity divided by the spacing between isentropic surfaces.

Potential vorticity is conserved in adiabatic, frictionless flow by an ideal fluid at all scales. In a tropical environment with active convection, PV will be conserved only in portions of that environment without active convection or precipitation. In the areas of convection, diabatic generation and destruction of PV will be proportional to the net transport of mass into or out of isentropic layers. Since heating (latent or otherwise) in isentropic coordinates causes transport of mass from cooler (lower) layers to warmer (higher) layers, the effect of deep convective heating is low-level generation and upper-level destruction of PV. In a sense, as the mass ascends, the PV descends.

When length and time scales are such that the wind and mass fields are able to remain close to balance (such as geostrophic balance, gradient wind balance, nonlinear balance, etc.), the three-dimensional distribution of PV determines the three-dimensional distribution of all other parameters such as temperature, pressure, etc. In the Northern Hemisphere a positive PV anomaly (which, for the sake of this discussion, we shall take to mean an area within an isentropic layer where the PV is larger than in the surrounding portions of that isentropic layer) will have both vorticity and stratification higher than its surroundings. Below and above the positive PV anomaly the vorticity will be high and stratification low relative to the horizontal surroundings; the magnitude of these effects are proportional to the strength of the PV anomaly and decay with distance from the PV anomaly. The air horizontally surrounding

the PV anomaly will have low vorticity and high stratification, again decaying with distance. Negative PV anomalies will be associated with atmospheric variations of the opposite sign.

The same balance constraints require that a balanced vorticity maximum at a particular level will have variations of temperature and stratification associated with it, and thus it will be host to a positive PV anomaly. Also, in moist-neutral tropical environments where a given isentropic layer is nearly flat and of uniform thickness, horizontal variations of vorticity of large magnitude directly imply large horizontal variations of PV.

If more than one PV anomaly is present, or the PV varies continuously, the resulting stratification, vorticity, etc. at any point in the atmosphere can be estimated by computing the combined effects of all nearby PV anomalies. The mathematical performance of this operation is called PV inversion.

A well-developed hurricane has a positive PV anomaly that is particularly strong at low levels and within the radius of maximum wind. This PV anomaly is overlaid by a much broader negative PV anomaly consisting of the outflow of air expelled through the updrafts of the hurricane. Hurricane genesis requires the creation (or assembly) of a low-level PV anomaly of sufficient magnitude that the winds associated with that PV anomaly (in approximate gradient wind balance) reach hurricane strength.

REFERENCES

Chen, S. S., and W. M. Frank, 1993: A numerical study of the genesis of extratropical convective mesovortices. Part I: Evolution and dynamics. *J. Atmos. Sci.,* **50,** 2401–2426.

Corbosiero, K. L., and J. Molinari, 2002: The effects of vertical wind shear on the distribution of convection in tropical cyclones. *Mon. Wea. Rev.,* **130,** 2110–2123.

Craig, G. C., and S. L. Gray, 1996: CISK or WISHE as the mechanism for tropical cyclone intensification. *J. Atmos. Sci.,* **53,** 3528–3540.

Davis, C., and L. F. Bosart, 2001: Numerical simulations of the genesis of Hurricane Diana (1984). Part I: Control simulation. *Mon. Wea. Rev.,* **129,** 1859–1881.

DeMaria, M., and J. M. Gross, 2003: Evolution of prediction models. *Hurricane! Coping with Disaster: Progress and Challenges since Galveston, 1900,* R. Simpson, Ed., Amer. Geophys. Union, 103–126.

——, J. A. Knaff, and B. H. Connell, 2001: A tropical cyclone genesis parameter for the tropical Atlantic. *Wea. Forecasting,* **16,** 219–233.

Emanuel, K. A., 1986: An air-sea interaction theory for tropical cyclones. Part I: Steady-state maintenance. *J. Atmos. Sci.,* **43,** 585–604.

——, 1989: The finite-amplitude nature of tropical cyclogenesis. *J. Atmos. Sci.,* **46,** 3431–3456.

——, 2003: A century of scientific progress: An evaluation. *Hurricane! Coping with Disaster: Progress and Challenges since Galveston, 1900,* R. Simpson, Ed., Amer. Geophys. Union, 177—204.

——, J. D. Neelin, and C. S. Bretherton, 1994: On large scale circulations in convecting atmospheres. *Quart. J. Roy. Meteor. Soc.,* **120,** 1111–1144.

Fritsch, J. M., J. D. Murphy, and J. S. Kain, 1994: Warm core vortex amplification over land. *J. Atmos. Sci.,* **51,** 1780–1807.

Gray, W. M., 1968: Global view of the origin of tropical disturbances and storms. *Mon. Wea. Rev.,* **96,** 669–700.

——, 1975: Tropical cyclone genesis. Dept. of Atmospheric Science Paper 323, Colorado State University, 121 pp. [Available from Department of Atmospheric Sciences, Colorado State University, Ft. Collins, CO 80523.]

Harr, P. A., R. L. Elsberry, and J. C. Chan, 1996: Transformation of a large monsoon depression to a tropical storm during TCM-93. *Mon. Wea. Rev.,* **124,** 2625–2643.

Haynes, P. H., and M. E. McIntyre, 1987: On the evolution of vorticity and potential vorticity in the presence of diabatic heating and frictional or other forces. *J. Atmos. Sci.,* **44,** 828–841.

——, and ——, 1990: On the conservation and impermeability theorems for potential vorticity. *J. Atmos. Sci.,* **47,** 2021–2031.

Hendricks, E. A., M. T. Montgomery, and C. A. Davis, 2004: The role of "vortical" hot towers in the formation of tropical cyclone Diana (1984). *J. Atmos. Sci.,* **61,** 1209–1232.

Hoskins, B. J., M. E. McIntyre, and A. W. Robertson, 1985: On the use and significance of isentropic potential vorticity maps. *Quart. J. Roy. Meteor. Soc.,* **111,** 877–946.

Malkus, J. S., C. Ronne, and M. Chaffee, 1961: Cloud patterns in Hurricane Daisy. *Tellus,* **13,** 8–30.

McBride, J. L., and R. Zehr, 1981: Observational analysis of tropical cyclone formation. Part II: Comparison of non-developing versus developing systems. *J. Atmos. Sci.,* **38,** 1132–1151.

Menard, R. D., and J. M. Fritsch, 1989: A mesoscale convective complex-generated inertially stable warm core vortex. *Mon. Wea. Rev.,* **117,** 1237–1261.

Molinari, J., S. Skubis, D. Vollaro, F. Alsheimer, and H. E. Willoughby, 1998: Potential vorticity analysis of tropical cyclone intensification. *J. Atmos. Sci.,* **55,** 2632–2644.

——, D. Vollaro, and K. L. Corbosiero, 2004: Tropical cyclone formation in a sheared environment: A case study. *J. Atmos. Sci.,* **61,** 2493–2509.

Montgomery, M. T., and J. Enagonio, 1998: Tropical cyclogenesis via convectively forced vortex Rossby waves in a three-dimensional quasigeostrophic model. *J. Atmos. Sci.,* **55,** 3176–3207.

——, M. E. Nichols, T. A. Cram, and A. Saunders, 2006: A vortical hot tower route to tropical cyclogenesis. *J. Atmos. Sci.,* **63,** 355–386.

Orlanski, I., 1975: The rational subdivision of scales for atmospheric processes. *Bull. Amer. Meteor. Soc.,* **56,** 527–530.

Raymond, D. J., and H. Jiang, 1990: A theory for long-lived mesoscale convective systems. *J. Atmos. Sci.,* **47,** 3067–3077.

Reasor, P. D., M. T. Montgomery, and L. F. Bosart, 2005: Mesoscale observations of the genesis of Hurricane Dolly (1996). *J. Atmos. Sci.,* **62,** 3151–3171.

Reihl, H., and J. S. Malkus, 1958: On the heat balance in the equatorial trough zone. *Geophysica,* **6,** 503–538.

Ritchie, E. A., and G. J. Holland, 1997: Scale interactions during the formation of Typhoon Irving. *Mon. Wea. Rev.,* **125,** 1377–1396.

Rogers, R. F., and J. M. Fritsch, 2001: Surface cyclogenesis from

convectively driven amplification of midlevel mesoscale convective vortices. *Mon. Wea. Rev.,* **129,** 605–637.

Rotunno, R., and K. A. Emanuel, 1987: An air–sea interaction theory for tropical cyclones. Part II: Evolutionary study using a nonhydrostatic axisymmetric numerical model. *J. Atmos. Sci.,* **44,** 542–561.

Shapiro, L. J., and J. L. Franklin, 1995: Potential vorticity in Hurricane Gloria. *Mon. Wea. Rev.,* **123,** 1465–1475.

Simpson, J., E. Ritchie, G. J. Holland, J. Halverson, and S. Stewart, 1997: Mesoscale interactions in tropical cyclone genesis. *Mon. Wea. Rev.,* **125,** 2643–2661.

——, B. Halverson, B. S. Ferrier, W. A. Peterson, R. H. Simpson, R. Blakeslee, and S. L. Durden, 1998: On the role of "hot towers" in tropical cyclone formation. *Meteor. Atmos. Phys.,* **67,** 15–35.

Spratt, S. M., D. W. Sharp, P. Welsh, A. Sandrik, F. Alsheimer, and C. Paxton, 1997: A WSR-88D assessment of tropical cyclone outer rainband tornadoes. *Wea. Forecasting,* **12,** 479–501.

Stewart, S. R., and S. W. Lyons, 1996: A WSR-88D radar view of Tropical Cyclone Ed. *Wea. Forecasting,* **11,** 115–132.

Stossmeister, G. J., and G. M. Barnes, 1992: The development of a second circulation center within Tropical Storm Isabel (1985). *Mon. Wea. Rev.,* **120,** 685–697.

Willoughby, H. E., 1990: Gradient balance in tropical cyclones. *J. Atmos. Sci.,* **47,** 265–274.